

Convergence Analysis for Computation of Coupled Advection-Diffusion-Reaction Problems

W. B. Dong¹, H. S. Tang^{1,*}, Y. J. Liu²

¹Civil Engineering Department, City College of New York, CUNY, New York, USA

²School of Mathematics, Georgia Institute of Technology, Atlanta, USA

ABSTRACT A study is presented on the convergence of the computation of coupled advection-diffusion-reaction equations. In the computation, the equations with different coefficients and even types are assigned in two subdomains, and Schwarz iteration is made between the equations when marching from a time level to the next one. The analysis starts with the linear systems resulting from the full discretization of the equations by explicit schemes. Conditions for convergence are derived, and its speedup and the effects of difference in the equations are discussed. Then, it proceeds to an implicit scheme, and a recursive expression for convergence speed is derived. An optimal interface condition for the Schwarz iteration is obtained, and it leads to “perfect convergence”, that is, convergence within two times of iteration. Furthermore, the methods and analyses are extended to the coupling of the viscous Burgers equations. Numerical experiments indicate that the conclusions, such as the “perfect convergence,” drawn in the linear situations may remain in the Burgers equations’ computation.

Keywords: Domain decomposition, advection-diffusion-reaction equation, the viscous Burgers equation, Scarborough criterion, optimized interface condition

1. Introduction

Advection, diffusion, and reaction are fundamental physical phenomena, which and whose interactions take place in real-world problems. These phenomena and interactions are described by advection-diffusion-reaction equations and their coupling, which have been solved numerically to understand such phenomena underlying various physical processes, such as migration of pollutants in a porous medium, chemical reaction in a nuclear reactor, and propagation of tsunamis in the ocean [1, 2, 3]. Additionally, more complicated partial differential equations (PDEs) and their coupling, such as the Navier-Stokes equations and their hydrostatic versions [4, 5], are adopted to simulate realistic multiscale/multiphysics problems. Since advection-diffusion-reaction equations exhibit behaviors of parabolic, hyperbolic, and elliptic equations, they are commonly used as models to study these complicated PDEs and their coupling [6, 7, 8, 9]. As a result, a study on the computation of coupled advection-diffusion-reaction equations promotes simulations of actual physical problems and the development of numerical methods for PDEs.

Domain decomposition (DD) has emerged as an indispensable avenue to the scientific computation of various problems, and its development in methods and analysis for coupled equations of advection, diffusion, and reaction can trace back over 30 years ago, e.g., [6, 10]. A natural approach of computation is to compute these equations in subdomains in conjunction with Schwarz iteration in between when marching from a time level to the next level [11, 12, 13]. This approach is widely used in practical problems such as simulation of fluid flows [14, 15]. Another popular approach is to adopt Schwarz waveform relaxation, by which at each time of Schwarz iteration the equations in subdomains are solved at all time levels [16, 17, 18]. Investigations have covered diffusion equations

*Correspondence: Hasnong Tang, htang@ccny.cuny.edu

[11, 16, 19], advection equations [20, 14, 21], advection-diffusion equations [22, 17, 23], heterogeneous advection-diffusion equations [24, 25], and other closely-related equations (e.g., the Darcy law, a fractional equation, and the Schrödinger equation) [12, 18, 26], all with or without reaction. The research topics include, algorithm study [27, 28, 13], convergence analysis [21, 29, 18, 13], interface conditions in heterogeneous problems (e.g., between an advection-diffusion equation and an advection equation) [6, 30, 12], and optimal transmission conditions [23, 17]. As a more general form of advection-reaction equations, hyperbolic systems of conservation laws have also been investigated intensively [31, 32], especially in the context of fluid flow simulation [33]. In the computation of the systems, explicit discretization is commonly used, and, therefore, no iteration between subdomains is needed. In such a situation, interface algorithms and stability issues have been a main research topic [32, 34, 35].

Progress has been made in understanding DD computation of coupled advection-diffusion-reaction equations. It is known that the convergence rate increases with the size of the overlapping region, decreases with diffusion coefficients, and gets slower as the grid spacing gets finer [23]. The convergence rate can be accelerated by methods such as precondition in iteration matrices and optimization for interface conditions, and such speedup can be over an order of magnitude [17, 10]. For systems of conservation laws, it is proven that, when conservative interface algorithms are adopted at grid interfaces, numerical solutions converge to weak solutions of the systems if they converge [32]. Then, it is shown that, under certain conditions that can be verified, even when non-conservative interface algorithms are used, still convergent solutions will become weak solutions, and the conservation errors are bounded [35]. Later, it is further proved that the conservation error tends to zero at the speed of $\mathcal{O}(\Delta t)$, regardless of the smoothness of solutions at the interfaces [36]. In the computation of the systems, discretization is necessary to avoid numerical oscillations, nonphysical solutions, and multiple solutions [34, 37, 38].

Despite the substantial study, more topics deserve investigation. Heterogeneous DD problems of advection-diffusion-reaction equations are such a topic. In the past, research has been focused on homogeneous problems, e.g., identical equations in subdomains, and investigations on heterogeneous problems are relatively sparse, although relevant efforts have been made previously [6, 30]. Additionally, previous analysis investigations are primarily conducted at the continuous level and semi-discretizations levels [39, 29]. While studies at such levels are successful and have revealed many important patterns of the problems, their results may not be conveniently or directly applied to practical computation. For instance, often the analysis of interface conditions is made based on the Laplace or Fourier transform, and the corresponding obtained optimal parameters are expressed in a spectral space and thus need to be approximated for actual computation [14, 40]. Moreover, most studies are about linear problems in the past, with scarce discussion on nonlinear equations.

This paper presents a systematic analysis of the computation of coupled advection-diffusion-reaction equations, and it intends to fill the gaps listed above and also deals with situations beyond those in existing work. Notably, such equations, with different coefficients in subdomains in general, are fully discretized using either explicit or implicit schemes. The analysis starts with explicit schemes for the computation of the resulting algebraic systems. Conditions for the convergence are derived, and its speedup and behaviors are examined, together with a discussion on the effects of difference in PDEs in subdomains. Then, the analysis proceeds to an implicit scheme and derivation of its convergence speed, followed by the derivation of its optimal interface algorithm. Finally, the study is extended to the coupling of the viscous Burgers equations, and analysis based on linearization is made on their computation.

2. The problem of study

This paper considers computation of the following initial value problem of coupled advection-diffusion-reaction equations in two subdomains:

$$\begin{cases} u_{1t} + f_x^1(u_1) = b_1 u_{1xx} - c_1 u_1, & x < x_2 \\ u_1 = u_2, & x = x_2 \\ u_1 = g(x), & t = 0 \end{cases} \quad \begin{cases} u_{2t} + f_x^2(u_2) = b_2 u_{2xx} - c_2 u_2, & x > x_1 \\ u_2 = u_1, & x = x_1 \\ u_2 = g(x), & t = 0 \end{cases} \quad (1)$$

in which t is the time, and x is the space coordinate. Subdomain 1 is on the left, $x \leq x_2$, and subdomain 2 is on the right, $x \geq x_1$. The two subdomains overlap with each other, i.e., $x_1 < x_2$, and $x = x_1$ and x_2 are the interface of subdomain 2 and 1, respectively. In this study, $f^k(u_k) = a_k u_k, u_k^2/2$ ($k = 1, 2$) will be considered. a_k, b_k , and c_k are constant coefficients, and their values may be different in the two subdomains. As a result, problem (1) includes a number of coupling scenarios, such as coupling between two advection-diffusion-reaction equations with different coefficient, between an advection-diffusion equation ($a_1, b_1, c_1 \neq 0$) and an advection equation ($b_2, c_2 = 0$), and an advection equation ($b_1, c_1 = 0$) and a diffusion-reaction equation ($a_2 = 0$). As seen in (1), Dirichlet conditions are used the interfaces. Moreover, boundary conditions at the left and right ends of subdomain 1 and 2, respectively, may be added. Without loss of generality, it is assume that $g(x)$ has a finite support.

Consider computation of problem (1) on two grids as shown in Fig.1, with the left and right grid covering subdomain 1 and 2, respectively. Node I of the left grid and node 1 of the right grid are the interfaces of the two grids, and they correspond to the interfaces of the two subdomains. On the two grids, the advection-diffusion-reaction equations are discretized with backward difference and central difference in time and space, respectively, and this leads to an implicit scheme:

$$\frac{u_{k_i}^{n+1} - u_{k_i}^n}{\Delta t} + f_{u_i}^{k,n+1} \frac{u_{k_{i+1}}^{n+1} - u_{k_{i-1}}^{n+1}}{2\Delta x} = b_k \frac{u_{k_{i+1}}^{n+1} - 2u_{k_i}^{n+1} + u_{k_{i-1}}^{n+1}}{\Delta x^2} - c_k u_{k_i}^{n+1} \quad (2)$$

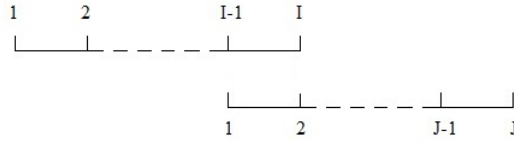


Figure 1: Computational grids. The left and right grids cover subdomain 1 and 2, respectively.

where $k = 1, 2$, depicting subdomain 1 and 2, respectively, Δt and Δx are the time step and the grid spacing, respectively, superscript n and subscript i indicate time level and grid node, respectively, and $f_u^k = \partial f^k(u_k)/\partial u_k$.

This paper aims to analyze convergence of the computation of discretization (2). The computation can be carried out by treating $u_{k_i}^{n+1}$ as $u_{k_i}^m$ and/or $u_{k_i}^{m+1}$, which leads to either explicit or implicit schemes (in terms of $u_{k_i}^{m+1}$) in the two subdomains, together with Schwarz iteration in between. Particularly, when marching from time level n to $n + 1$ via an explicit scheme, the

problem will be solved as ($m = 0, 1, 2, \dots$):

$$\begin{cases} \mathcal{F}(\dots, u_{1_i}^m, \dots, u_{1_i}^{m-1}, \dots, u_{1_i}^n, \dots) = 0, & u_{1_I}^m = u_{2_1}^m \\ \mathcal{F}(\dots, u_{2_i}^m, \dots, u_{2_i}^{m-1}, \dots, u_{2_i}^n, \dots) = 0, & u_{2_1}^m = u_{1_{I-1}}^m \end{cases} \quad (3)$$

Here, \mathcal{F} represents an iterative scheme to compute discretization (2) in subdomains. As $m \rightarrow \infty$, if convergent, the iterated solution converges to the solution at time level $n + 1$: $u_{1_i}^m \rightarrow u_{1_i}^{n+1}$, $u_{2_i}^m \rightarrow u_{2_i}^{n+1}$. In above, the two grids exchange solutions at a same level of iteration, i.e. m , at their interfaces, and this is possible when an explicit iterative scheme is adopted in subdomains. When an implicit scheme is used, the exchange will be made between different levels of iteration: $u_{1_I}^m = u_{2_1}^{m-1}$, and $u_{2_1}^m = u_{1_2}^{m-1}$. Such interface conditions, with solution exchange either at a same or at a different level, are Dirichlet conditions, and they are referred to as classic interface conditions hereafter.

Note that, instead of (2), the equations may be discretized using an explicit scheme, but this study focuses on an implicit scheme given its advantages such as better numerical stability and wide use in practical computation. Moreover, it is readily checked that the discretization accuracy of (2) is $\mathcal{O}(\Delta t + \Delta x^2)$. If needed, $\mathcal{O}(\Delta t^2 + \Delta x^2)$ can be achieved, for instance, by discretizing the time derivative with a second-order accurate, three-time-level backward difference (e.g., [15]), or, discretizing the whole equation with the Crank-Nicholson scheme (e.g., [36]). However, the analysis of (2) in this paper remains the same or similar when these types of discretization are considered. At last, instead of that by waveform relaxation, this work considers the computation by Schwarz iteration only within two adjacent time levels n and $n + 1$, which is commonly adopted, especially in practical problem [15, 13].

3. Explicit scheme

3.1 Preliminary

Consider a linear system

$$AU = b \quad (4)$$

in which $A = (a_{ij})$, $U = (u_i)$, and $b = (b_i)$, with $i, j = 1, 2, \dots, N$. When the system is solved by the Jacobi iteration, one has ($m = 1, 2, \dots$)

$$U^m = (I - D^{-1}A)U^{m-1} + D^{-1}b \quad (5)$$

in which I is the identity matrix, and D is a diagonal matrix with the diagonal elements of A as its diagonal elements. A theorem shown by Saad in [41] shows that (5) converges as long as

$$\sum_{i=1, \neq j}^N |a_{ij}| / |a_{ii}| \begin{cases} \leq 1, & j = 1, \dots, N \\ < 1, & \text{at least one } j \end{cases} \quad (6)$$

and A is irreducible. Instead of above, the following condition is frequently used as a sufficient

condition for convergence of (5) in practical computation, e.g., heat and mass transfer [42, 43]:

$$\sum_{j=1, \neq i}^N |a_{ij}|/|a_{ii}| \begin{cases} \leq 1, & i = 1, \dots, N \\ < 1, & \text{at least one } i \end{cases} \quad (7)$$

which is proposed by Scarborough [44, 45], and is referred to as the Scarborough criterion [42, 43]. Note that, the summation in condition (6) is over rows, while that in the Scarborough criterion is over columns.

Remark 3.1 In the work of Scarborough [45], criterion (7) is proposed but not actually proved, and in fact condition (6) is proved instead, all without "=". The theorem shown by Saad in [41] (Theorem 4.9) actually leads to a proof for the Scarborough criterion. Actually, by the theorem, Scarborough criterion (7) is a convergence condition for iteration $U^m = (I - D^{-1}A)^T U^{m-1}$. As a result, the spectral radius of $(I - D^{-1}A)^T$ is less than 1, and thus the spectral radius of $(I - D^{-1}A)$ must be less than 1 also since their radius are the same. As a result, iteration (5) converges under the Scarborough criterion.

The following is a trivial case for a more general conclusion. Given an iteration

$$U^m = CU^{m-1} + d \quad (8)$$

where $C = (c_{ij})$, and $d = (d_i)$, with $i, j = 1, 2, \dots, N$. Let

$$K = \max_i \left\{ \sum_{j=1}^L |c_{ij}| \right\} = \|C\|_\infty \quad (9)$$

In view that $\|C\| < 1$ leads to the convergence of the iteration, $K < 1$, or, the following

$$\sum_{j=1}^N |c_{ij}| < 1 \quad (10)$$

for every i , is a condition for the convergence.

3.2 Condition for convergence

Consider computation of (3) by iterative, explicit schemes in the two subdomains. Two common explicit schemes will be considered, and the first one reads as ($k = 1, 2$)

$$\frac{u_k^m - u_k^n}{\Delta t} + a_k \frac{u_{k+1}^{m-1} - u_{k-1}^{m-1}}{2\Delta x} = b_k \frac{u_{k+1}^{m-1} - 2u_k^m + u_{k-1}^{m-1}}{\Delta x^2} - c_k u_k^m, \quad (11)$$

which is iterative and actually the Jacobi iteration [46]. This scheme is simple and slow in convergence, but it permits parallel computation and is in frequent use for practical problems [42, 43]. With this scheme, Schwarz iteration (3) reads as

$$\begin{cases} (1 + 2\epsilon_1 + \gamma_1)u_1^m = (\eta_1 + \epsilon_1)u_{1-1}^{m-1} + (\epsilon_1 - \eta_1)u_{1+1}^{m-1} + u_1^n, & i \leq I - 1; & u_1^m = u_2^m \\ (1 + 2\epsilon_2 + \gamma_2)u_2^m = (\eta_2 + \epsilon_2)u_{2-1}^{m-1} + (\epsilon_2 - \eta_2)u_{2+1}^{m-1} + u_2^n, & i \geq 2; & u_2^m = u_1^m \end{cases} \quad (12)$$

in which $\eta_k = a_k \Delta t / (2\Delta x)$, $\epsilon_k = b_k \Delta t / \Delta x^2$, and $\gamma_k = \Delta t c_k$ ($k = 1, 2$). By arranging terms, above iteration can be expressed as (5), in which

$$A = \left[\begin{array}{ccc|ccc} \ddots & \ddots & \ddots & & & \\ & r_1 & s_1 & t_1 & & \\ & & r_1 & s_1 & & \\ \hline & & & r_2 & t_2 & \\ & & & & s_2 & t_2 \\ & & & & & \ddots \\ & & & & & \ddots \end{array} \right], \quad U = \begin{bmatrix} \vdots \\ u_{1I-2} \\ u_{1I-1} \\ u_{22} \\ u_{23} \\ \vdots \end{bmatrix}, \quad b = \begin{bmatrix} \vdots \\ u_{1I-2}^n \\ u_{1I-1}^n \\ u_{22}^n \\ u_{23}^n \\ \vdots \end{bmatrix}$$

in which $r_k = -\epsilon_k - \eta_k$, $s_k = 1 + 2\epsilon_k + \gamma_k$, $t_k = \eta_k - \epsilon_k$. By Scarborough principle (7), the following is concluded.

PROPOSITION 3.1 A sufficient condition for iteration (12) to converge is

$$\max_k \left\{ \frac{|\epsilon_k + \eta_k| + |\eta_k - \epsilon_k|}{|1 + 2\epsilon_k + \gamma_k|} \right\} < 1 \quad (13)$$

Now, let us discuss if (13) is, or, how to make it satisfied. In view that $\eta_k = a_k \Delta t / (2\Delta x)$, $\epsilon_k = b_k \Delta t / \Delta x^2$, and $\gamma_k = \Delta t c_k$, it is readily seen that, the LHS of (13) decreases with Δt , and, as Δt becomes sufficiently small, (13) will be guaranteed. Additionally, it is seen that the LHS also decreases with γ_k . Note that the LHS is K , or, $\|C\|_\infty$, see (9). In view that $\rho(C) \leq \|C\|_\infty$, a small value of Δt and a large value of γ_i lead to a smaller K and thus are helpful to assure the convergence.

The coefficients of the PDEs may be different in the two subdomains. For instance, when $\epsilon_1, \gamma_1, \gamma_2 = 0$, the coupling becomes one between an advection equation and a advection-diffusion equation. In this scenario, the LHS becomes

$$K = \max \left\{ \left| \frac{2\eta_1}{1 + 2\epsilon_1} \right|, \frac{|\epsilon_2 + \eta_2| + |\eta_2 - \epsilon_2|}{|1 + 2\epsilon_2|} \right\}$$

which will be less than 1 as long as Δt is sufficiently small, as discussed above. Another scenario is $\eta_k = 0$, that is, the problem becomes coupling between two diffusion equations. Because $\epsilon_k, \gamma_k > 0$, one has

$$K = \max_k \left| \frac{2\epsilon_k}{1 + 2\epsilon_k + \gamma_k} \right| < 1$$

or, (13) holds automatically. Discussion for more scenarios can be made.

Another iterative, explicit algorithm is the so-called artificial compressibility method, which is a main approach used in computation of incompressible flow problems [47, 36]. By this approach, an artificial term is added, and the discretization reads as

$$\frac{u_{k_i}^m - u_{k_i}^{m-1}}{\Delta \tau} + \frac{u_{k_i}^m - u_{k_i}^n}{\Delta t} + a_k \frac{u_{k_{i+1}}^{m-1} - u_{k_{i-1}}^{m-1}}{2\Delta x} = b_k \frac{u_{k_{i+1}}^{m-1} - 2u_{k_i}^{m-1} + u_{k_{i-1}}^{m-1}}{\Delta x^2} - c_k u_{k_i}^{m-1} \quad (14)$$

in which $\Delta \tau$ is a pseudo-time step. At the convergence, the artificial term disappears. While the

artificial compressibility method is adopted, the Schwarz iteration becomes

$$\left\{ \begin{array}{l} (1 + \kappa)u_{1_i}^m = (\eta_1 + \epsilon_1)u_{1_{i-1}}^{m-1} + (\kappa - 2\epsilon_1 - \gamma_1)u_{1_i}^{m-1} + (\epsilon_1 - \eta_1)u_{1_{i+1}}^{m-1} + u_{1_i}^n, \\ \quad i \leq I - 1; \quad u_{1_I}^m = u_{2_2}^m \\ (1 + \kappa)u_{2_i}^m = (\eta_2 + \epsilon_2)u_{2_{i-1}}^{m-1} + (\kappa - 2\epsilon_2 - \gamma_2)u_{2_i}^{m-1} + (\epsilon_2 - \eta_2)u_{2_{i+1}}^{m-1} + u_{2_i}^n, \\ \quad i \geq 2; \quad u_{2_1}^m = u_{2_{I-1}}^m \end{array} \right. \quad (15)$$

where $\kappa = \Delta t / \Delta \tau$. Above can be formulated into form of iteration (8). In this situation, C is a tri-diagonal matrix, and, from the left to the right in a row, its non-zero elements are $r_k = (\epsilon_k + \eta_k) / (1 + \kappa)$, $s_k = (\kappa - (2\epsilon_k + \gamma_k)) / (1 + \kappa)$, $t_k = (\epsilon_k - \eta_k) / (1 + \kappa)$, together with $d = (u_{1_2}^n / (1 + \kappa), \dots, u_{1_{I-1}}^n / (1 + \kappa), u_{2_2}^n / (1 + \kappa), \dots, u_{2_{I-1}}^n / (1 + \kappa))^T$. According to (10), we have the following conclusion.

PROPOSITION 3.2 A sufficient condition for (15) to converge is

$$\max_k \left\{ \left| \frac{\epsilon_k + \eta_k}{1 + \kappa} \right| + \left| \frac{\kappa - (2\epsilon_k + \gamma_k)}{1 + \kappa} \right| + \left| \frac{\epsilon_k - \eta_k}{1 + \kappa} \right| \right\} < 1 \quad (16)$$

Now, let us also examine if (16) can be satisfied. Actually, (16) will hold as long as $\Delta \tau$ is sufficiently small. This is because in this situation, when $\epsilon_k \geq \eta_k$, its LHS becomes

$$K = \max_k \left| \frac{\kappa - \gamma_k}{1 + \kappa} \right| < 1$$

When $\epsilon_k < \eta_k$, it is easy to check that

$$K = \max_k \left| \frac{\kappa - (2(\epsilon_k - \eta_k) + \gamma_k)}{1 + \kappa} \right| < 1$$

Discussions can be made for more possible scenarios.

3.3 Analysis of convergence speed

Convergence speed Introducing relaxation into the interface condition in (12), one has

$$\begin{aligned} u_{1_I}^m &= u_{2_2}^{m-1} + \omega_1(u_{2_2}^m - u_{2_2}^{m-1}) \\ u_{2_1}^m &= u_{1_{I-1}}^{m-1} + \omega_2(u_{1_{I-1}}^m - u_{1_{I-1}}^{m-1}) \end{aligned}$$

where $\omega_1, \omega_2 = \text{consts}$, being the relaxation coefficients. With such an interface condition, the Jacobi iteration (5) is formulated as (8), in which

$$C = \left[\begin{array}{ccc|ccc} \ddots & \ddots & \ddots & & & \\ & r_1 & 0 & t_1 & & \\ & 0 & 0 & 0 & \omega_1 r_2 & (1 - \omega_1) & \omega_1 t_2 \\ \hline \omega_2 r_1 & (1 - \omega_2) & \omega_2 t_1 & 0 & 0 & 0 \\ & & & r_2 & 0 & t_2 \\ & & & & \ddots & \ddots & \ddots \end{array} \right], \quad U = \left[\begin{array}{c} \vdots \\ u_{1_{I-1}} \\ u_{1_I} \\ u_{2_1} \\ u_{2_2} \\ \vdots \end{array} \right]$$

and $r_k = (\epsilon_k + \eta_k)/(1 + 2\epsilon_k + \gamma_k)$, $t_k = (\epsilon_k - \eta_k)/(1 + 2\epsilon_k + \gamma_k)$. According to condition (10), a sufficient condition for convergence is

$$\max_{k,k'} \left\{ |\omega_k| \left(\left| \frac{\epsilon_{k'} + \eta_{k'}}{1 + 2\epsilon_{k'} + \gamma_{k'}} \right| + \left| \frac{\epsilon_{k'} - \eta_{k'}}{1 + 2\epsilon_{k'} + \gamma_{k'}} \right| \right) + |1 - \omega_k| \right\} < 1$$

where $k, k' = 1, 2$, and $k \neq k'$. Note that the LHS becomes the summation of the other rows without $\omega_k, \omega_{k'}$ in C when $\omega_k, \omega_{k'} = 1$. As discussed above, it is anticipated that the convergence of the iteration may become faster as K becomes smaller. It is readily checked that $\partial K / \partial \omega_k < -1$, > -1 , and > 1 when $\omega_k \leq 0$, $0 < \omega_k \leq 1$, and $\omega_k > 1$, respectively. It is expected that K will have a minimum within $0 \leq \omega_k \leq 1$, and, particularly, at either $\omega_k = 0$, or, $= 1$, which correspond to interface condition $u_{1I}^m = u_{22}^{m-1}$, $u_{21}^m = u_{1I-1}^{m-1}$ and that in (12), respectively.

As a numerical experiment, three cases shown in Table 1 are computed. The three cases represent typical situations of problem (1). Particularly, Case 1, 2, and 3 involve coupling between two diffusion-dominant equations, between two advection-dominant equations, and between a diffusion-dominant and an advection-dominant equation, respectively. The result is given in Table 2, which shows that spectral radius, ρ , for $\omega_k = 1$ is lower than that for $\omega_k = 0$, exhibiting a faster convergence.

Table 1: Cases for numerical experiments on linear advection-diffusion-reaction equations.

Case	a_1	b_1	c_1	a_2	b_2	c_2
1	0.01	0.5	0.0	0.01	0.5	0.0
2	0.5	0.002	0.0	0.25	0.001	0.0
3	0.25	0.01	0.25	-0.25	0.01	0.5

Table 2: Spectral radii of the Jacobi iteration associated with the relaxation interface condition. (I,J)=(40,80).

Case	$\omega_1, \omega_2 = 0$	$\omega_1, \omega_2 = 1$
1	0.967363	0.966594
2	0.267145	0.197162
3	0.431927	0.359324

Now, let us consider the convergence of artificial compressibility method (15) in association with different values for κ . For above three cases, K , together with ρ , at different values of κ are plotted in Fig. 2. It is seen that in all of the three cases, K takes the smallest value at $\omega_k = 1$. Additionally, K is a good indicator for the value of ρ , and both of them take the lowest values at about a same κ . Therefore, in practical computation, choosing a value of κ at the smallest K tends to lead to the smallest ρ , which corresponds to the fast convergence speed.

Dependence of convergence speed on grid spacing and time step Let us look into the convergence speed and start with two identical equations in subdomains. It is seen in above that the iteration matrices for the Jacobi method and the artificial compressibility method are tridiagonal.

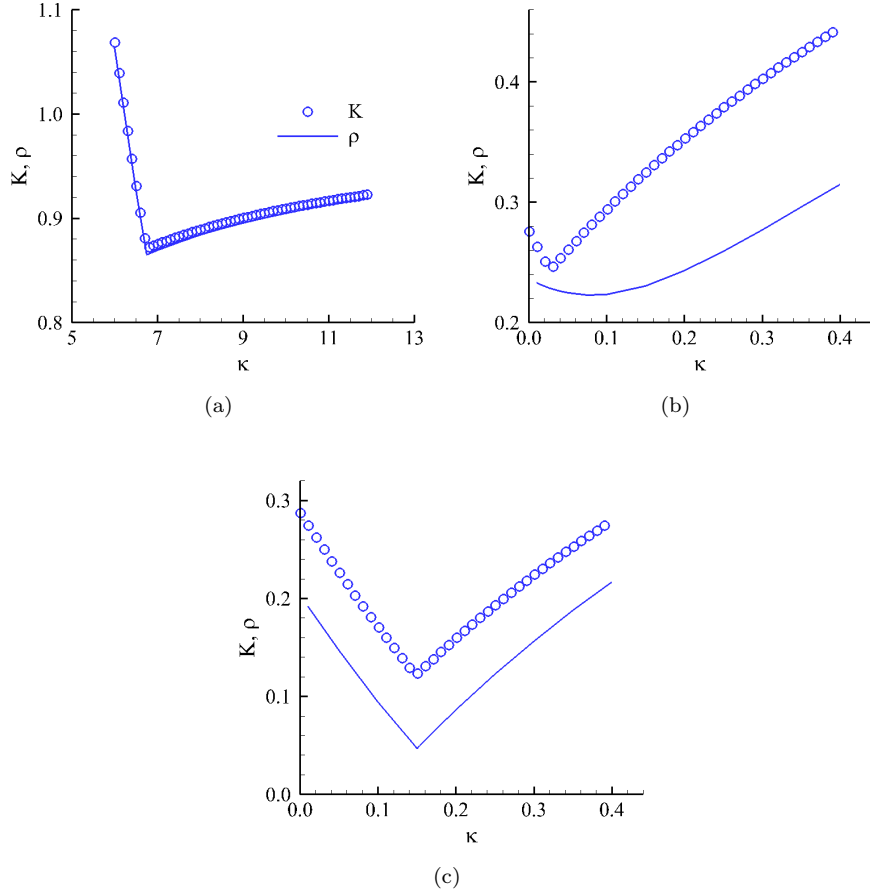


Figure 2: Correlation of K and ρ in the artificial compressible method. a) Case 1. b) Case 2. c) Case 3.

For an $N \times N$ tridiagonal matrix with elements p_{-1} , p_0 , p_1 , its eigenvalues read as [48]

$$\lambda_i = p_0 - 2\cos\left(\frac{i\pi}{N+1}\right)\sqrt{p_{-1}p_1}, \quad i = 1, 2, \dots, N \quad (17)$$

by which, the spectral radius of the Jacobi method becomes

$$\rho = 2\cos\left(\frac{N\pi}{N+1}\right)\frac{\sqrt{\epsilon_k^2 - \eta_k^2}}{1 + 2\epsilon_k + \gamma_k}$$

Let $\epsilon_k = \text{const}$ and $\epsilon_k \geq \eta_k$, the latter of which is always true when grid spacing is sufficiently small. Then, as $\Delta t, \Delta x$ decrease, the term of “cos” increases, and η_k and γ_k decreases, leading to increase in the term of fraction. As a result, ρ increases monotonically as $\Delta t, \Delta x$ decrease, with an upper limit of $2\epsilon_k/(1 + 2\epsilon) < 1$, and this is seen in Case 1 and 3 in Fig. 3a. If $\eta_k = \text{const}$ and $\epsilon_k < \eta_k$,

as the mesh gets finer, the term of fraction does not increase or even decreases, and this may lead to no increase or even a decrease in the spectral radius. A numerical example is Case 2 in the figure. All of these indicate that, in some situations, the spectral radius, or, the convergence speed, is scalable with mesh resolution. Note that the radius may increase again at much finer grids. Similar discussion may be made for the artificial compressibility method, for which the spectral radius becomes

$$\rho = \frac{\kappa - (2\epsilon_k + \gamma_k)}{1 + \kappa} + \frac{2}{1 + \kappa} \cos\left(\frac{N\pi}{N+1}\right) \sqrt{\epsilon_k^2 - \eta_k^2}$$

Again, the spectral radius may be scalable in terms of grid spacing when κ takes certain values, and numerical examples are shown in Fig. 3b. Note that, in studies of waveform relaxation methods, it is concluded that convergence rates deteriorate as grid spacing decrease, e.g., [16].

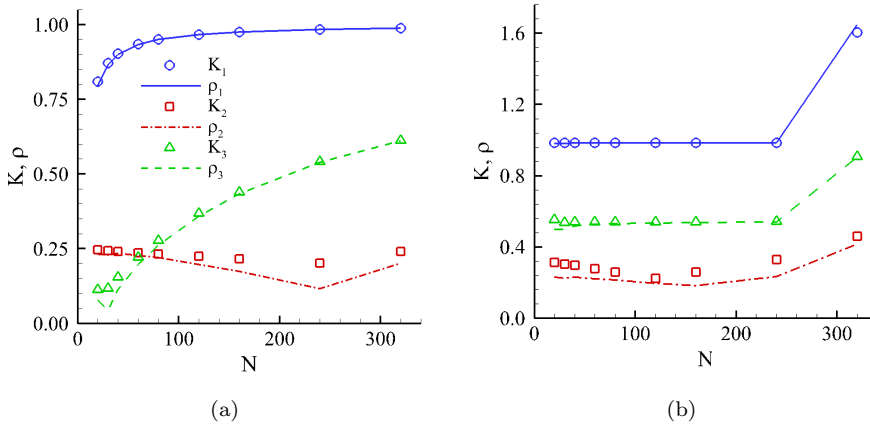


Figure 3: Spectral radius at different mesh resolution. Subscripts for K and ρ indicate the case numbers. $N = I + J - 4$, I and J are the number of grid nodes in subdomain 1 and 2, respectively. $(I, J) = (10, 10), (10, 20), (20, 20), (20, 40), (40, 40), (40, 80), (80, 80), (80, 160), (160, 160)$. $\Delta t/\Delta x = 0.5$. a) The Jacobi method. b) The compressibility method. $\kappa = 59.25, 0.19$, and 1.19 for Case 1, 2, and 3, respectively.

Outer and inner iteration If an iterative scheme is adopted in the subdomains, two types of iteration are involved when marching from time level n to $n + 1$: one is the iteration within subdomains, referred to as the inner iteration, and the other is the Schwarz iteration between them, called the outer iteration. Such a situation is commonly encountered in computation of realistic problems, e.g., [15]. To illustrate the computation, Jacobi iteration (12) is modified as

$$\begin{cases} (1 + 2\epsilon_1 + \gamma_1)u_1^l = (\eta_1 + \epsilon_1)u_{1,i-1}^{l-1} + (\epsilon_1 - \eta_1)u_{1,i+1}^{l-1} + u_1^n, & l = 1, 2, \dots, L; i \leq I - 1; \\ u_1^l = u_2^{m-1} \\ (1 + 2\epsilon_2 + \gamma_2)u_2^l = (\eta_2 + \epsilon_2)u_{2,i-1}^{l-1} + (\epsilon_2 - \eta_2)u_{2,i+1}^{l-1} + u_2^n, & l = 1, 2, \dots, L; i \geq 2; \\ u_2^l = u_{1,i-1}^{m-1} \end{cases} \quad (18)$$

in which l is the inner iteration index, and m is the outer iteration index. After inner iteration fully converges, $u_{1,i}^l \rightarrow u_{1,i}^m$, $u_{2,i}^l \rightarrow u_{2,i}^m$. Similar formulation can also be made for the artificial compressibility method. A natural question in computation of (18) will be how to arrange the inner

Table 3: Computational load with different combinations of the inner and outer iteration. ‘1:1’, means after one outer iteration, one inner iteration is made, and ‘conver.’ indicates that after one outer iteration, inner iteration keeps going until convergence. The computational load is defined as the times of computation in each subdomain, or, the total number of times of inner iteration in each subdomain, together with convergence tolerance of 10^{-12} .

Case	1:1	1:5	1:15	conver.
1	8	43	102	131
2	8	43	111	147
3	8	43	115	152

and outer iteration to achieve fast convergence, or, after how many times of inner iteration an outer iteration should be started to achieve a minimal count of computational load.

It is not straightforward to theoretically answer the above question, and a numerical experiment is made to achieve a preliminary understanding. Particularly, computation is made for the three cases in Table 1 in association with the following initial and boundary conditions

$$g(x) = -\sin(\pi x), \quad t = 0; \quad u_1 = 0, \quad x = -1, \quad u_2 = 0, \quad x = 1 \quad (19)$$

In the experiment, the corresponding conditions for convergence, i.e., (13) and (16), are satisfied. Also, the computation starts the outer iteration after every 1, 5, and 15 times of the inner iteration, and also after complete convergence of the inner iteration. The results are presented in Table 3. Note that in the computation, for each case, the difference in computational load mainly comes from the numbers of inner iteration, while its number of outer iteration remains about the same. The table shows that the earlier the outer iteration starts, the smaller the amount of computational load. More particularly, the 1:1 strategy is the best; the computation that starts an outer iteration after every inner iteration spends the least amount of computational load.

4. Implicit scheme

4.1 Convergence speed

An implicit scheme to compute (2) in the subdomains reads as

$$\frac{u_{ki}^m - u_{ki}^n}{\Delta t} + a_k \frac{u_{k,i+1}^m - u_{k,i-1}^m}{2\Delta x} = b_k \frac{u_{k,i+1}^m - 2u_{ki}^m + u_{k,i-1}^m}{\Delta x^2} - c_k u_{ki}^m \quad (20)$$

Together with the interface condition, the computation can be formulated as

$$\begin{cases} (\eta_1 + \epsilon_1)u_{1,i-1}^m + (1 + 2\epsilon_1 + \gamma_1)u_{1,i}^m + (\epsilon_1 - \eta_1)u_{1,i+1}^m + u_{1,i}^n, & i \leq I - 1; & u_{1I}^m = u_{22}^{m-1} \\ (\eta_2 + \epsilon_2)u_{2,i-1}^m + (1 + 2\epsilon_2 + \gamma_2)u_{2,i}^m + (\epsilon_2 - \eta_2)u_{2,i+1}^m + u_{2,i}^n, & i \geq 2; & u_{21}^m = u_{1I-1}^{m-1} \end{cases} \quad (21)$$

The computation in each subdomain needs to solve a linear system. At convergence, $u_{1,i}^m$ and $u_{2,i}^m$ become $u_{1,i}^{n+1}$ and $u_{2,i}^{n+1}$, respectively. In terms of residual, i.e., $e_{1,i}^m = u_{1,i}^m - u_{1,i}^{n+1}$ and $e_{2,i}^m = u_{2,i}^m - u_{2,i}^{n+1}$, above computation becomes

$$\begin{cases} -(\eta_1 + \epsilon_1)e_{1,i-1}^m + (1 + 2\epsilon_1 + \gamma_1)e_{1,i}^m - (\eta_1 - \epsilon_1)e_{1,i+1}^m = 0, & i \leq I - 1; & e_{1I}^m = e_{21}^{m-1} \\ -(\eta_2 + \epsilon_2)e_{2,i-1}^m + (1 + 2\epsilon_2 + \gamma_2)e_{2,i}^m - (\eta_2 - \epsilon_2)e_{2,i+1}^m = 0, & i \geq 2; & e_{21}^m = e_{1I-1}^{m-1} \end{cases} \quad (22)$$

PROPOSITION 4.1 The contraction factor of computation (22) is a recursive expression:

$$\bar{\rho} = \frac{(\eta_1 - \epsilon_1)(\eta_2 + \epsilon_2)}{R_1(I-2)R_2(2)} \quad (23)$$

where $\bar{\rho} = e_{1_i}^{m+2}/e_{1_i}^m, e_{2_i}^{m+2}/e_{2_i}^m$ and

$$\begin{aligned} R_1(i) &= 1 + 2\epsilon_1 + \gamma_1 + \frac{\eta_1^2 - \epsilon_1^2}{R_1(i-1)}; \quad i = 3, \dots, I-1; \quad R_1(2) = 1 + 2\epsilon_1 + \gamma_1 \\ R_2(j) &= 1 + 2\epsilon_2 + \gamma_2 + \frac{\eta_2^2 - \epsilon_2^2}{R_2(j+1)}; \quad j = J-2, \dots, 2; \quad R_2(J-1) = 1 + 2\epsilon_2 + \gamma_2 \end{aligned} \quad (24)$$

in which $I, J \geq 3$.

Proof: The proposition can be proved by the induction method. The two equations in (22) when $i = 2, 3$ are

$$\begin{aligned} (1 + 2\epsilon_1 + \gamma_1)e_{1_2}^m + (\eta_1 - \epsilon_1)e_{1_3}^m &= 0 \\ -(\eta_1 + \epsilon_1)e_{1_2}^m + (1 + 2\epsilon_1 + \gamma_1)e_{1_3}^m + (\eta_1 - \epsilon_1)e_{1_4}^m &= 0 \end{aligned}$$

In above, without loss of generality (e.g., $g(x)$ in (1) has a finite support), $e_{1_1}^m, e_{2_3}^m = 0$ are used. It is readily derived the following by elimination of $e_{1_2}^m$ in above two equations:

$$(1 + 2\epsilon_1 + \gamma_1 + \frac{\eta_1^2 - \epsilon_1^2}{R_1(2)})e_{1_3}^m + (\eta_1 - \epsilon_1)e_{1_4}^m = 0$$

Then, continue above derivation, for instance, from the above equation and the equation in (22) when $i = 4$ in subdomain 1. It is expected that

$$\left(1 + 2\epsilon_1 + \gamma_1 + \frac{\eta_1^2 - \epsilon_1^2}{R_1(I-3)}\right)e_{1_{I-2}}^m + (\eta_1 - \epsilon_1)e_{1_{I-1}}^m = 0$$

The equation (22) in subdomain 1 when $i = I-1$ is

$$-(\eta_1 + \epsilon_1)e_{1_{I-2}}^m + (1 + 2\epsilon_1 + \gamma_1)e_{1_{I-1}}^m + (\eta_1 - \epsilon_1)e_{1_I}^m = 0$$

Using the two equations and noticing that the first parenthesis in the former is actually $R_1(I-2)$, it is readily derived that

$$\left(1 + 2\epsilon_1 + \gamma_1 + \frac{\eta_1^2 - \epsilon_1^2}{R_1(I-2)}\right)e_{1_{I-1}}^m + (\eta_1 - \epsilon_1)e_{1_I}^m = 0$$

which, after substitution of the interface conditions in (22) and change of index m in the latter, becomes

$$\left(1 + 2\epsilon_1 + \gamma_1 + \frac{\eta_1^2 - \epsilon_1^2}{R_1(I-2)}\right)e_{2_1}^{m+2} + (\eta_1 - \epsilon_1)e_{2_2}^m = 0$$

Similarly, starting from the two equations in subdomain 2 when $i = J - 1, J - 2$, one can derived that

$$-(\eta_2 + \epsilon_2)e_{21}^m + \left(1 + 2\epsilon_2 + \gamma_2 + \frac{\eta_2^2 - \epsilon_2^2}{R_2(2)}\right)e_{22}^m = 0$$

Above two equations results in (23) when $\bar{\rho} = e_{21}^{m+2}/e_{21}^m$. Moreover, from the latter, it is readily check that $e_{22}^{m+2}/e_{22}^m = e_{21}^{m+2}/e_{21}^m$. Also, as seen in above proof, the relation like the latter equation holds at $i > 2$, too. These indicate that (23) is true at all i in subdomain 1. In the same way, one can prove above for subdomain 1. These completes the proof.

Remark 4.1 Since the contraction factor is the same at all nodes, it is readily seen that such factor is actually the global convergence speed, e.g., $\bar{\rho} = \|e_{1i}^{m+2}\|_2/\|e_{1i}^m\|_2$.

In order to validate the derived convergence rate (23), a numerical experiment is made in computation of the three cases in Table 1 in conjunction with initial and boundary conditions (19). The theoretical contraction factor from (23) and numerical one computed directly from the solutions of the experiment are listed in Table 4, which shows that the two factors are basically identical, validating the derived one.

Table 4: Theoretical and numerical convergence speeds. $(I, J) = (40, 80)$, $\Delta t, \Delta x = 0.0171$.

Cases	$\bar{\rho}_{theo}$	$\bar{\rho}_{num}$
1	0.691235	0.691197
2	-0.017007	-0.017007
3	0.082962	0.082962

4.2 Optimal interface condition

In order to speed up convergence in computation of (21), the following optimal interface condition is adopted:

$$\begin{aligned} (u_{1I}^m - u_{1I-1}^m) + \alpha u_{1I}^m &= (u_{22}^{m-1} - u_{21}^{m-1}) + \alpha u_{22}^{m-1} \\ (u_{22}^m - u_{21}^m) + \beta u_{21}^m &= (u_{1I}^{m-1} - u_{1I-1}^{m-1}) + \beta u_{1I-1}^{m-1} \end{aligned} \quad (25)$$

in which $\alpha, \beta = const.$ Such optimal interface condition was first proposed for waveform relaxation of circuit problems by Gander et al., and it was effective in speeding up the convergence [49]. They show that, if $(\alpha + 1)(\beta - 1) + 1 \neq 0$, the optimal interface condition recovers to the classic condition, i.e., the interface condition in (21), at convergence as $m \rightarrow \infty$. Also, obviously, the optimal condition returns to the classic condition as $\alpha, \beta \rightarrow \infty$.

With the optimal interface condition, (22) is modified as

$$\begin{cases} -(\eta_1 + \epsilon_1)e_{1i-1}^m + (1 + 2\epsilon_1 + \gamma_1)e_{1i}^m - (\eta_1 - \epsilon_1)e_{1i+1}^m = 0, & i \leq I - 1 \\ (e_{1I}^m - e_{1I-1}^m) + \alpha e_{1I}^m = (e_{22}^{m-1} - e_{21}^{m-1}) + \alpha e_{21}^{m-1} \\ -(\eta_2 + \epsilon_2)e_{2i-1}^m + (1 + 2\epsilon_2 + \gamma_2)e_{2i}^m - (\eta_2 - \epsilon_2)e_{2i+1}^m = 0, & i \geq 2 \\ (e_{22}^m - e_{21}^m) + \beta e_{21}^m = (e_{1I}^{m-1} - e_{1I-1}^{m-1}) + \beta e_{1I-1}^{m-1} \end{cases} \quad (26)$$

The convergence speed for computation of (26) can be derived by following the same method and steps adopted to those in computation of (22), and this is based on a fact that the grid nodes involved in the former are exactly same as those in the latter. The derived results are summarized as follows.

PROPOSITION 4.2 The contraction factor in computation of (26) is

$$\bar{\rho} = -\frac{(\alpha + 1)(\eta_2 + \epsilon_2) - R_2(2)}{(\alpha + 1)R_1(I - 1) + \eta_1 - \epsilon_1} \cdot \frac{(\beta - 1)(\eta_1 - \epsilon_1) - R_1(I - 1)}{(\beta - 1)R_2(2) + \eta_2 + \epsilon_2} \quad (27)$$

in which $I, J \geq 3$.

In expression (27), letting the numerators be zero while keeping denominators be non-zero leads to zero contraction factor, i.e., $\bar{\rho} = 0$, and the following optimal α and β :

$$\alpha = \frac{R_2(2)}{\eta_2 + \epsilon_2} - 1, \quad \beta = \frac{R_1(I - 1)}{\eta_1 - \epsilon_1} + 1 \quad (28)$$

together with condition $R_1(I - 1)R_2(2) + (\eta_1 - \epsilon_1)(\eta_2 + \epsilon_2) \neq 0$. From (27) and (28), it is derived that

$$\begin{aligned} \frac{\partial \bar{\rho}}{\partial \alpha} &= -\frac{R_1(I - 1)R_2(2) + (\eta_1 - \epsilon_1)(\eta_2 + \epsilon_2)}{[(\alpha + 1)R_1(I - 1) + (\eta_1 - \epsilon_1)]^2} \cdot \frac{(\beta - 1)(\eta_1 - \epsilon_1) - R_1(I - 1)}{(\beta - 1)R_2(2) + (\eta_2 + \epsilon_2)} \\ \frac{\partial \bar{\rho}}{\partial \beta} &= -\frac{(\alpha + 1)(\eta_2 + \epsilon_2) - R_2(2)}{(\alpha + 1)R_1(I - 1) + (\eta_1 - \epsilon_1)} \cdot \frac{R_1(I - 1)R_2(2) + (\eta_1 - \epsilon_1)(\eta_2 + \epsilon_2)}{[(\beta - 1)R_2(2) + (\eta_2 + \epsilon_2)]^2} \end{aligned}$$

additionally,

$$\begin{aligned} \frac{\partial^2 \bar{\rho}}{\partial \alpha^2} &= -\frac{2R_1(I - 1)[R_1(I - 1)R_2(2) + (\eta_1 - \epsilon_1)(\eta_2 + \epsilon_2)]}{[(\alpha + 1)R_1(I - 1) + (\eta_1 - \epsilon_1)]^3} \cdot \frac{(\beta - 1)(\eta_1 - \epsilon_1) - R_1(I - 1)}{(\beta - 1)R_2(2) + (\eta_2 + \epsilon_2)} \\ \frac{\partial^2 \bar{\rho}}{\partial \beta^2} &= -\frac{(\alpha + 1)(\eta_2 + \epsilon_2) - R_2(2)}{(\alpha + 1)R_1(I - 1) + (\eta_1 - \epsilon_1)} \cdot \frac{2R_2(2)[R_1(I - 1)R_2(2) + (\eta_1 - \epsilon_1)(\eta_2 + \epsilon_2)]}{[(\beta - 1)R_2(2) + (\eta_2 + \epsilon_2)]^3} \\ \frac{\partial^2 \bar{\rho}}{\partial \alpha \partial \beta} &= -\frac{[R_1(I - 1)R_2(2) + (\eta_1 - \epsilon_1)(\eta_2 + \epsilon_2)]^2}{[(\alpha + 1)R_1(I - 1) + (\eta_1 - \epsilon_1)]^2[(\beta - 1)R_2(2) + (\eta_2 + \epsilon_2)]^2} \end{aligned}$$

Under conditions (28), it is readily verified that

$$\begin{aligned} \frac{\partial \bar{\rho}}{\partial \alpha} &= 0, \quad \frac{\partial \bar{\rho}}{\partial \beta} = 0 \\ \frac{\partial^2 \bar{\rho}}{\partial \alpha^2} &= 0, \quad \frac{\partial^2 \bar{\rho}}{\partial \beta^2} = 0, \quad \frac{\partial^2 \bar{\rho}}{\partial \alpha \partial \beta} \neq 0 \end{aligned}$$

As a result, one has

$$\frac{\partial^2 \bar{\rho}}{\partial \alpha^2} \frac{\partial^2 \bar{\rho}}{\partial \beta^2} - \left(\frac{\partial^2 \bar{\rho}}{\partial \alpha \partial \beta} \right)^2 < 0$$

With above, it is known that (α, β) given by (28) is a saddle point of $\bar{\rho}$ [50]. All above proves the following theorem.

THEOREM 4.1 At the optimal value of (α, β) given in (28), the contraction factor (27) is zero.

Moreover, the optimal value of (α, β) is a saddle point of $\bar{\rho}$.

Remark 4.2 Actually, contraction factor (27) becomes zero when either α takes the value in (28), regardless that of β , or, β takes the value in (28), regardless that of α . Also, the zero contraction factor occurs only when (α, β) are given as (28).

Remark 4.3 The past work is at the continuous or semi-discretization level, and its optimal values for (α, β) can only be derived in a transformed space. As a result, search and approximation for them at the algebraic level have to be made in actual computation, e.g., [40]. As a distinct feature in this study, the optimal (α, β) can be directly computed by (28), without any approximation. Therefore, the derived theoretical convergence speed exactly matches that in practical computation, as shown in the following numerical examples.

Again, a numerical experiment is made on the three cases in Table 1 with initial and boundary conditions (19), and the results are shown in Table 5. The table shows that, at the optimal values for (α, β) , the numerical contraction factors in the numerical solutions are very small or almost zeros. These factors are not exactly zero, which is the theoretical value, and this is attributed to the lack of enough accuracy in the computer. Calculations indicate that the value of $\bar{\rho}$ is subtle to the values of α and β , or, enough digits should be kept in calculation of (28) to achieve zero for a contraction factor. To directly illustrate the effectiveness of the optimal interface condition, the convergence residuals in the experiment are shown in Fig. 4a. The figure shows that, in comparison to the classic condition, the optimal condition greatly speeds up the convergence. In view that the contraction factor is the ratio of residual between two subsequent times of iteration, a zero convergence factor implies that convergence will be achieved with no more than two times of convergence. The figure shows that indeed the convergence is achieved in about two times of iteration. Moreover, Fig. 4b illustrates a distribution of the contraction factor on the α - β plane, and it clearly shows that the values of α and β given by (28) is a saddle point.

Table 5: Optimal (α, β) and convergence speed. (I,J)=(40,80), $\Delta t, \Delta x = 0.017$.

Cases	$\alpha,$	β	$\bar{\rho}_{num}$
1	$2.02577 \times 10^{-1},$	-2.02988×10^{-1}	1.31×10^{-14}
2	$5.14615 \times 10^0,$	1.05666×10^1	-6.12×10^{-15}
3	$1.74955 \times 10^0,$	-3.38389×10^0	0

5. Extension to Burgers' equation

5.1 Explicit scheme

Consider the coupling between two viscous Burgers' equations with reaction terms. Now the discretization (2) becomes

$$\frac{u_{k_i}^{n+1} - u_{k_i}^n}{\Delta t} + u_{k_i}^{n+1} \frac{u_{k_{i+1}}^{n+1} - u_{k_{i-1}}^{n+1}}{2\Delta x} = b_k \frac{u_{k_{i+1}}^{n+1} - 2u_{k_i}^{n+1} + u_{k_{i-1}}^{n+1}}{\Delta x^2} - c_k u_{k_i}^{n+1}, \quad (29)$$

which can be computed with an extension of (11), i.e., the Jacobi method for the linear advection-diffusion-reaction equation, particularly, by letting its a_k be replaced by $u_{k_i}^{m-1}$. With such an extension, computation of above discretization in association with the classic interface condition

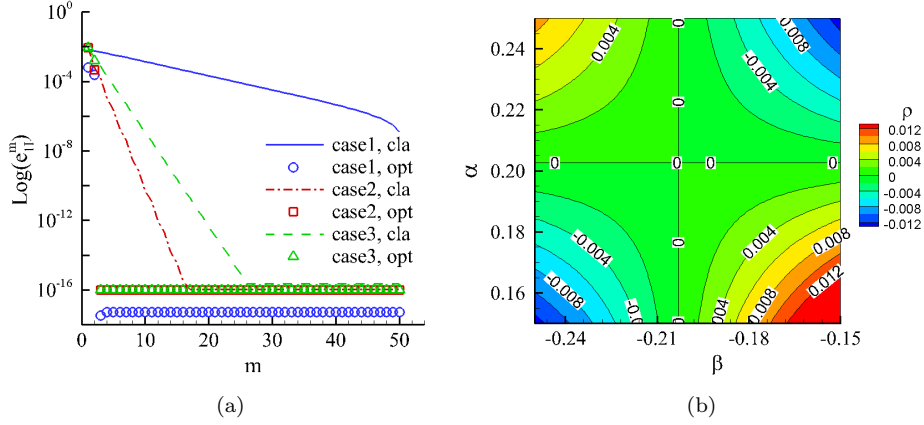


Figure 4: Computation with optimal interface condition. a) Convergence processes. b) Contraction factor. Case 1, $(I, J) = (40, 80)$.

leads to an explicit algorithm

$$\begin{cases} (1 + 2\epsilon_1 + \gamma_1)u_{1i}^m = (\eta_{1i}^{m-1} + \epsilon_1)u_{1i-1}^{m-1} + (\epsilon_1 - \eta_{1i}^{m-1})u_{1i+1}^{m-1} + u_{1i}^n, & i \leq I-1; \\ u_{1I}^m = u_{22}^m \\ (1 + 2\epsilon_2 + \gamma_2)u_{2i}^m = (\eta_{2i}^{m-1} + \epsilon_2)u_{2i-1}^{m-1} + (\epsilon_2 - \eta_{2i}^{m-1})u_{2i+1}^{m-1} + u_{2i}^n, & i \geq 2; \\ u_{21}^m = u_{1I-1}^m \end{cases} \quad (30)$$

A difference of above iteration from the previous iteration is that now the value of η becomes solution dependent. In order to analyze above iteration, linearization is made by replacing its η_{ki}^{m-1} with $\eta_{ki}^n = \Delta t u_{ki}^n / (2\Delta x)$ ($k = 1, 2$). As a result, the iteration between the two time levels can be formulated in form of (12) with η_k be replaced by η_{ki}^n , and the associated coefficient matrix A remains constant during the iteration while marching from time level n to $n+1$. According to the Scarborough criterion, the following conclusion is achieved (Note that LHS is not a constant but changes with i, n).

PROPOSITION 5.1 A sufficient condition for the linearized version of (30) to converge is

$$\max_{i,k} \left\{ \frac{|\epsilon_k + \eta_{ki}^n| + |\eta_{ki}^n - \epsilon_k|}{|1 + 2\epsilon_k + \gamma_k|} \right\} < 1 \quad (31)$$

Discretization (29) can also be computed using the artificial compressibility method, and this is realized by replacing a_k with u_{ki}^{m-1} in (14). Consequently, method (15) is extended as

$$\begin{cases} (1 + \kappa)u_{1i}^m = (\eta_{1i}^{m-1} + \epsilon_1)u_{1i-1}^{m-1} + (\kappa - 2\epsilon_1 - \gamma_1)u_{1i}^{m-1} + (\epsilon_1 - \eta_{1i}^{m-1})u_{1i+1}^{m-1} + u_{1i}^n, \\ i \leq I-1; u_{1I}^m = u_{22}^m \\ (1 + \kappa)u_{2i}^m = (\eta_{2i}^{m-1} + \epsilon_2)u_{2i-1}^{m-1} + (\kappa - 2\epsilon_2 - \gamma_2)u_{2i}^{m-1} + (\epsilon_2 - \eta_{2i}^{m-1})u_{2i+1}^{m-1} + u_{2i}^n, \\ i \geq 2; u_{21}^m = u_{1I-1}^m \end{cases} \quad (32)$$

By linearization to replace η_{ki}^{m-1} with η_{ki}^n ($k = 1, 2$) and with a similar discussion, the following is obtained.

PROPOSITION 5.2 A sufficient condition for the linearized version of (32) to converge is

$$\max_{i,k} \left\{ \left| \frac{\epsilon_k + \eta_{1_i}^n}{1 + \kappa} \right| + \left| \frac{\kappa - (2\epsilon_k + \gamma_k)}{1 + \kappa} \right| + \left| \frac{\epsilon_k - \eta_{k_i}^n}{1 + \kappa} \right| \right\} < 1 \quad (33)$$

The analysis for computation of (30) and (32) can be made similarly as in Section 3.3 for the linear advection-diffusion-reaction equations. As an illustration of the analysis, numerical experiments are made on four cases in Table 6. Case 4 and 5 are respectively diffusion and advection dominated, respectively, and Case 6 and 7 are a combination of them. Initial and boundary conditions in (19) are used in Case 4 and 7. For case 5 and 6, the initial condition becomes piecewise: $g(x) = 1, x \in [-0.5, 0.5]$, $g(x) = 0, x \in [-1, -0.5], (0.5, 1]$.

Table 6: Cases for numerical experiments on the viscous Burgers equations.

Cases	b_1	c_1	b_2	c_2
4	0.5	0.0	0.5	0.0
5	0.02	2.0	0.02	3.0
6	0.1	0.2	0.2	0.1
7	0.5	0.0	0.51	0.0

Table 7 presents the values for LHS of (31) and (33), together with those for the spectral radii. It is seen that when these two conditions are satisfied, all radii are less than 1, and thus convergence in these linearized versions of (30) and (32) is guaranteed. Noted that since the equations become nonlinear, particularly, in general, $\eta_{k_i}^n$ changes with solutions, and its values are distinct at different time steps. To illustrate this, results at three moments in time are presented in the table. In computation of (32), effects of κ on K and ρ are plotted in Fig. 5. Again, it is seen that the value of κ corresponding to the lowest K is a good approximation of its value for the lowest ρ , which results in the fastest convergence.

Table 7: LHS of (31) and (33), and corresponding spectral radius. (I,J)=(10,20), $\Delta t, \Delta x = 0.0741$. For the artificial compressibility method, $\kappa = 1.350, 0.069, 0.542$, and 1.378 are used in Case 4, 5, 6, and 7, respectively. These values of κ correspond to the lowest values of K , as shown in Fig. 5.

Time	0.074		0.222		0.370	
	K	ρ	K	ρ	K	ρ
Jacobi, 4	0.574468	0.558299	0.574468	0.566377	0.574468	0.568848
Jacobi, 5	0.080057	0.055298	0.057561	0.041587	0.050176	0.044854
Jacobi, 6	0.350481	0.340231	0.350481	0.342112	0.350481	0.343251
Jacobi, 7	0.574468	0.572429	0.574468	0.573695	0.574468	0.574239
Artificial, 4	0.574468	0.568429	0.574468	0.569622	0.574468	0.570135
Artificial, 5	0.081437	0.054665	0.058767	0.047987	0.051325	0.041229
Artificial, 6	0.635802	0.623317	0.635802	0.625591	0.635802	0.626952
Artificial, 7	0.597447	0.589117	0.597447	0.590465	0.597447	0.591051

Lastly, let us look into the issue of inner and outer iteration, and extend Jacobi iteration (18) by replacing η_k with $\eta_{k_i}^{l-1}$. The results of computation for the cases in Table 6 are presented in Table

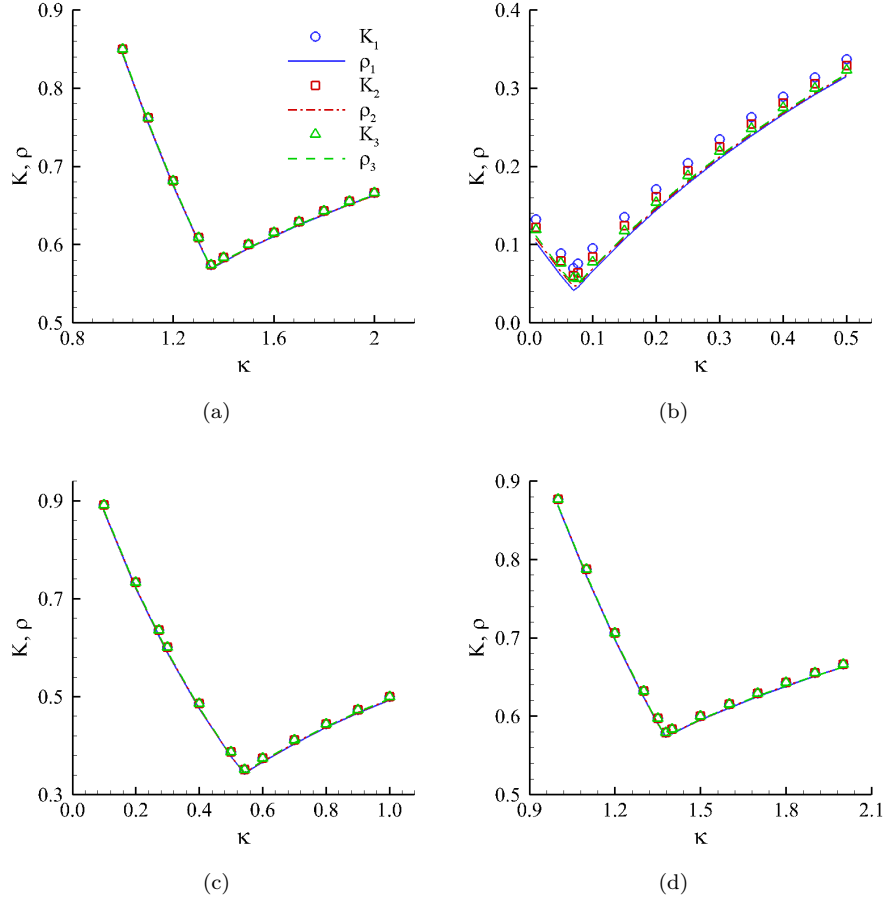


Figure 5: Correlation of K and ρ in the artificial compressible method for the Burgers equations. Subscript 1, 2, and 3 indicate $t=0.074, 0.222,$ and $0.370,$ respectively. a) Case 4. b) Case 5. c) Case 6. d) Case 7.

8, and they show a same trend observed in the linear advection-diffusion-reaction equations. Particularly, the earlier to start the outer iteration, the smaller the computational load, or, the quicker the overall convergence. The smallest computational load occurs at the 1:1 strategy. Therefore, an understanding is that the 1:1 strategy leads to the fastest convergence in the examples of this paper, regardless the equations are linear or nonlinear. Such a strategy has been used in practical problems [15].

5.2 Implicit scheme

Now consider computation of discretization (29) by an implicit scheme, and this is realized by replacing its a_k with $u_{k_i}^{m-1}$ in scheme (20). With such modification, the computational problem

Table 8: Computational load associated with different combinations of the inner and outer iteration, for the Burgers equations, together with convergence tolerance of 10^{-12} , at $t = 0.170$.

Case No.	1:1	1:5	1:15	conver.
4	7	63	72	120
5	9	70	86	132
6	8	66	78	125
7	7	62	72	120

becomes

$$\left\{ \begin{array}{l} (\eta_{1i}^{m-1} + \epsilon_1)u_{1i-1}^m + (1 + 2\epsilon_1 + \gamma_1)u_{1i}^m + (\epsilon_1 - \eta_{1i}^{m-1})u_{1i+1}^m + u_{1i}^n, \quad i \leq I-1; \\ u_{1I}^m = u_{2I}^{m-1} \\ (\eta_{2i}^{m-1} + \epsilon_2)u_{2i-1}^m + (1 + 2\epsilon_2 + \gamma_2)u_{2i}^m + (\epsilon_2 - \eta_{2i}^{m-1})u_{2i+1}^m + u_{2i}^n, \quad i \geq 2; \\ u_{21}^m = u_{1I-1}^{m-1} \end{array} \right. \quad (34)$$

which requires to solve linear systems in subdomains at each iteration over m .

Let us analyze computation of (34) by linearization with η_{1i}^{m-1} and η_{2i}^{m-1} being replaced by η_{1i}^n and η_{2i}^n , respectively. As a result, (34) becomes a linear iterative scheme. Follow the proof of Proposition 4.1, still a contraction factor can be derived on the basis of linearization as follows.

PROPOSITION 5.3 The contraction factor for computing the linearized Burgers equations, (34), is

$$\bar{\rho} = \frac{(\eta_{1I-1}^n - \epsilon_1)(\eta_{22}^n + \epsilon_2)}{R_1(I-1)R_2(2)} \quad (35)$$

where $\bar{\rho} = e_{1i}^{m+2}/e_{1i}^m$, $\bar{\rho} = e_{2i}^{m+2}/e_{2i}^m$, and

$$\begin{aligned} R_1(i) &= 1 + 2\epsilon_1 + \gamma_1 + \frac{(\eta_{1i-1}^n - \epsilon_1)(\eta_{1i}^n + \epsilon_1)}{R_1(i-1)}; \quad i = 3, \dots, I-1, \quad R_1(2) = 1 + 2\epsilon_1 + \gamma_1 \\ R_2(j) &= 1 + 2\epsilon_2 + \gamma_2 + \frac{(\eta_{2j}^n - \epsilon_2)(\eta_{2j+1}^n + \epsilon_2)}{R_2(j+1)}; \quad j = J-2, \dots, 2, \quad R_2(J-1) = 1 + 2\epsilon_2 + \gamma_2 \end{aligned} \quad (36)$$

in which $I, J \geq 3$.

From (35), it is seen that, same to (23), the contraction factor is the same in the two subdomains and at all grid nodes. However, the factor is related to η_{1i}^n and η_{2j}^n , and thus it changes at different time steps. Computation of (34) is made in association with the previous four cases. The contraction factor calculated from the numerical solutions and the theoretical one obtained from (35) are presented in Table 9, from which it is seen that they are close. The difference is attributed to the linearization adopted in the derivation of the theoretical contraction factor.

Now consider the computation of (34) but in association with optimal interface condition (25). Similarly to Proposition 4.2, the following is concluded.

PROPOSITION 5.4 When interface condition (25) is adopted, the contraction factor for compu-

Table 9: Theoretical and numerical contraction factors. $(I,J)=(40,80)$, $\Delta t, \Delta x = 0.017$.

Time	0.085		0.170		0.255	
Case	$\bar{\rho}_{theo}$	$\bar{\rho}_{num}$	$\bar{\rho}_{theo}$	$\bar{\rho}_{num}$	$\bar{\rho}_{theo}$	$\bar{\rho}_{num}$
4	0.689514	0.689539	0.690238	0.690248	0.690612	0.690608
5	0.295124	0.295112	0.299041	0.299082	0.302137	0.302190
6	0.457115	0.473308	0.462127	0.478952	0.466882	0.483229
7	0.702824	0.691392	0.703828	0.692029	0.704226	0.692274

tation of the linearized Burgers equations is

$$\bar{\rho} = -\frac{(\alpha + 1)(\eta_2^n + \epsilon_2) - R_2(2)}{(\alpha + 1)R_1(I - 1) + (\eta_1^n - \epsilon_1)} \cdot \frac{(\beta - 1)(\eta_1^n - \epsilon_1) - R_1(I - 1)}{(\beta - 1)R_2(2) + (\eta_2^n + \epsilon_2)} \quad (37)$$

where $I, J \geq 3$.

THEOREM 5.1 The contraction factor (37) becomes zero when

$$\alpha = \frac{R_2(2)}{\eta_2^n + \epsilon_2} - 1, \quad \beta = \frac{R_1(I - 1)}{\eta_1^n - \epsilon_1} + 1 \quad (38)$$

in association with $R_1(I - 1)R_2(2) + (\eta_1^n - \epsilon_1)(\eta_2^n + \epsilon_2) \neq 0$. In addition, above values of (α, β) is a saddle point of the contraction factor.

Proof: The proof can be made by following the steps for Theorem 4.1.

Numerical results for the four cases in Table 6 are presented in Table 10. It is seen that, when the optimal values for (α, β) in (38) are adopted, the actual contraction factors in the computation of the first two cases are almost zero, or the theoretical values, while they are somewhat away from zero in the rest two cases. The convergence residual is plotted in Fig. 6. The figure shows that, again, computation of the first two cases exhibits the “perfect convergence”, that is, it converges within about two times of iteration. In the rest two cases, the speed of convergence slows down, and the computation with the optimal interface condition needs many more times of iteration. However, it is still much faster than that associated with the classic interface condition. In the numerical experiment, it is noticed that the slowdown in convergence, as in the last two cases, happens once the diffusion coefficients b_1 and b_2 become different, even slightly. The reason for the slow down needs further investigation.

6. Concluding remarks

A study is presented on the computation of two coupled advection-diffusion-reaction equations. The research starts with the computation of the equations by explicit schemes. Then, it proceeds to an implicit scheme and speedup of convergence by an optimal interface condition. Further, the study is extended to coupled Burgers equations. This study achieves the following main results.

1. Conditions are presented for convergence of the computation by explicit schemes, and they are easy to use and check in practical problems. Also, such conditions bear clues to speed up convergence.

2. When an implicit scheme is adopted, an expression for convergence speed is derived. Addi-

Table 10: Convergence speed in computation of the Burgers equations, together with the optimized interface condition (25). $(I, J)=(40,80)$, $\Delta t, \Delta x = 0.017$.

Case	Time	α ,	β	$\bar{\rho}_{num}$
4	0.085	1.90740×10^{-1} ,	-2.17642×10^{-1}	-1.25×10^{-14}
	0.170	1.94634×10^{-1} ,	-2.12571×10^{-1}	8.63×10^{-15}
	0.255	1.97387×10^{-1} ,	-2.09199×10^{-1}	6.46×10^{-15}
5	0.085	6.09587×10^{-1} ,	-0.99418×10^{-1}	$0.00 \times 10^{+0}$
	0.170	6.37715×10^{-1} ,	-0.37090×10^{-1}	-1.69×10^{-14}
	0.255	6.66389×10^{-1} ,	-9.82950×10^{-1}	$0.00 \times 10^{+0}$
6	0.085	7.58689×10^{-1} ,	-4.29258×10^{-1}	9.44×10^{-2}
	0.170	7.62619×10^{-1} ,	-1.64360×10^{-1}	7.72×10^{-2}
	0.255	7.67611×10^{-1} ,	-9.94238×10^{-1}	6.31×10^{-2}
7	0.085	2.39686×10^{-1} ,	-1.47483×10^{-1}	-1.64×10^{-2}
	0.170	2.44286×10^{-1} ,	-1.41768×10^{-1}	-1.67×10^{-2}
	0.255	2.46275×10^{-1} ,	-1.39353×10^{-1}	-1.68×10^{-2}

tionally, an optimal interface condition is presented, which leads to “perfect convergence”, that is, convergence after two times of iteration.

3. Conclusions drawn in the above linear situations remain mostly true in the situations of the Burgers equations, such as the speedup by the optimal interface condition.

This study sheds light in understanding the computation of coupled advection-diffusion-reaction equations. For instance, this study confirms that convergence becomes slower as grid spacing gets fine, e.g., Fig. 3, which is concluded in computation by waveform relaxation methods. However, it observes that the convergence speed may not increase or even decrease with grid spacing in a wide range of parameters. Additionally, numerical evidence indicates that the overall convergence speed becomes the fastest if an outer iteration is made after every inner iteration, e.g., Table 3 and 8. Moreover, unlike those obtained in the transformed spaces in the continuous and semi-discretization levels, the convergence speeds’ expressions are explicit, and they directly predict those in actual computation. Actually, the method to derive these convergence speeds is extendable to other situations; we have derived the speeds for Poisson equations, which will be reported in a separate paper.

Some topics deserve further study. One of them is to extend the work of this paper to high dimensions in space, it would be more significant if successful. Another topic will be to understand why the convergence rate with an optimal interface condition remains ”perfect” in some scenarios of the Burgers equations, while it slows down substantially in some others. Theoretical analysis will be interesting on the relationship between inner and outer iteration, and why and under what conditions the 1:1 strategy leads to the fastest convergence. It will be interesting to compare the approach in this work,i.e., adopting Schwarz iteration while marching between two adjacent time levels, and that of waveform relaxation. All of these are potential topics of future study.

Acknowledgments. This work is supported by NSF (DMS # 1622453, # 1622459).

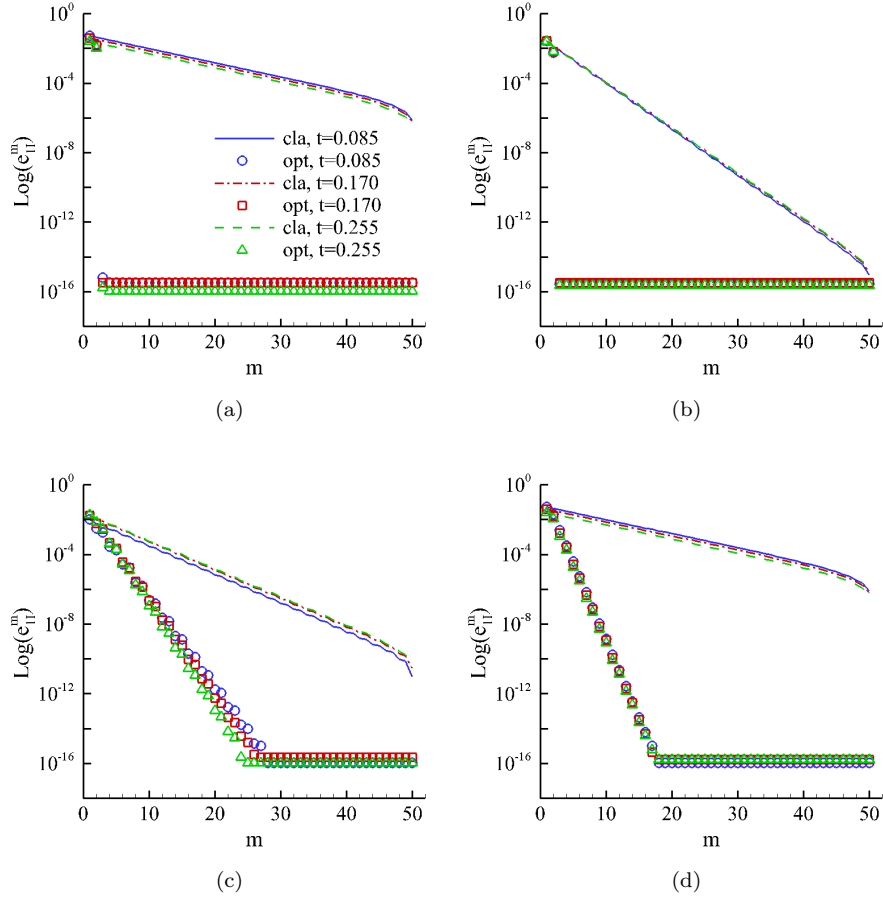


Figure 6: Computation with optimal interface conditions for the Burgers equations. a) Case 4. b) Case 5. c) Case 6. d) Case 7.

References

- [1] S. Atis, S. Saha, H. Auradou, J. Martin, N. Rakotomalala, L. Talon, and D. Salin. CHEMO-hydrodynamic coupling between forced advection in porous media and self-sustained chemical waves. *Chaos*, 22:037108, 2012.
- [2] S. Hamilton, M. Berrill, K. Clarno, R. Pawlowski, A. Toth, C. T. Kelley, T. Evans, and B. Philip. An assessment of coupling algorithms for nuclear reactor core physics simulations. *J. Comput. Phys.*, 311:241–257, 2016.
- [3] K. Qu, H.S. Tang, and A. Agrawal. Integration of fully 3D fluid dynamics and geophysical fluid dynamics models for multiphysics coastal ocean flows: Simulation of local complex free-surface phenomena. *Ocean Modelling*, 135:14–30, 2019.

- [4] H. S. Tang, K. Qu, and X. G. Wu. An overset grid method for integration of fully 3D fluid dynamics and geophysical fluid dynamics models to simulate multiphysics coastal ocean flows. *J. Comput. Phys.*, 273:548–571, 2014.
- [5] E. Blayo and A. Rousseau. About interface conditions for coupling hydrostatic and nonhydrostatic Navier-Stokes flows. *Discrete and Continuous Dynamical Systems Series*, 9:1565–1574, 2016.
- [6] F. Gastaldi and A. Quarteroni. On the coupling of hyperbolic and parabolic systems: Analytical and numerical approach. *Applied Numerical Mathematics*, 6:3–31, 1989/90.
- [7] H. Sakamoto, T. Hattori, A. Tada, and H. Nguyen, V. and Kawano. Analysis of Navier-Stokes equation from the viewpoint of advection diffusion. *Journal of Robotics, Networking and Artificial Life*, 1(4):265 – 269, 2015.
- [8] A. Main and G. Scovazzi. The shifted boundary method for embedded domain computations. Part II: Linear advection-diffusion and incompressible Navier-Stokes equations. *J. Comput. Phys.*, 372:996–1026, 2018.
- [9] J. Manzanero, E. Ferrer, G. Rubio, and E. Valero. Design of a Smagorinsky spectral vanishing viscosity turbulence model for discontinuous Galerkin methods. *Computers & Fluids*, 200:104440, 2020.
- [10] M. J. Gander. Schwarz methods over the course of time. *Electronic Transactions on Numerical Analysis*, 31:228–255, 2008.
- [11] G. A. Meurant. A domain decomposition method for parabolic problems. *Applied Numerical Mathematics*, 8:427–441, 1991.
- [12] T-T.P. Hoang, C. Japhet, M. Michel Kern, and J. E. Roberts. Space–time domain decomposition for advection–diffusion problems in mixed formulation. *Mathematics and Computers in Simulation*, 137:366–389, 2017.
- [13] C. Canuto and A. L. Giudice. A multi-timestep Robin–Robin domain decomposition method for time dependent advection-diffusion problems. *Applied Mathematics and Computation*, 363:124596, 2019.
- [14] V. Dolean, S. Lanteri, and F. Nataf. Optimized interface conditions for domain decomposition methods in fluid dynamics. *International Journal for Numerical Methods in Fluids*, 40(12):1539–1550, 2002.
- [15] H. S. Tang, C. Jones, and F. Sotiropoulos. An overset grid method for 3D unsteady incompressible flows. *J. Comput. Phys.*, 191:567–600, 2003.
- [16] M. J. Gander and A. M. Stuart. Space-time continuous analysis of waveform relaxation for the heat equation. *SIAM J. Sci. Comput.*, 19(6):2014–2031, 1998.
- [17] V. Martin. An optimized schwarz waveform relaxation method for the unsteady convection diffusion equation in two dimensions. *Computers & Fluids*, 33:829–837, 2004.
- [18] G. Califano and D. Conte. Optimal Schwarz waveform relaxation for fractional diffusion-wave equations. *Applied Numerical Mathematics*, 127:125–141, 2018.

- [19] P. Linel and P. Tromeur-Dervout. Analysis of the time-Schwarz DDM on the heat PDE. *Computers & Fluids*, 80:94–101, 2013.
- [20] A. Bamberger, R. Glowinski, and Q. H. Tran. A domain decomposition method for the acoustic wave equation with discontinuous coefficients and grid change. *SIAM Journal on Numerical Analysis*, 34(2):603–639, 1997.
- [21] V. Dolean and M. J. Gander. *Why classical schwarz methods applied to certain hyperbolic systems converge even without overlap*. U. Langer, M. Discacciati, D. Keyes, O. Widlund, W. Zulehner. In: Domain Decomposition Methods in Science and Engineering XVII. Lecture Notes in Computational Science and Engineering, 60 . Springer, AUT, pp. 467-475. ISBN 9783540751984, 2008.
- [22] E. Giladi and H. B. Keller. Space-time domain decomposition for parabolic problems. *Numer. Math.*, 93:279–313, 2002.
- [23] M. J. Gander and L. Halpern. Optimized Schwarz waveform relaxation methods for advection diffusion problems. *SIAM J. Numer. Anal.*, 45:666–697, 2007.
- [24] M. J. Gander¹, L. Halpern, and M. Kern. *A Schwarz Waveform Relaxation Method for Advection–Diffusion–Reaction Problems with Discontinuous Coefficients and Non-matching Grids*. Widlund O.B., Keyes D.E. (eds). In: Domain Decomposition Methods in Science and Engineering XXI. Lecture Notes in Computational Science and Engineering, 55. Springer, Berlin, Heidelberg., 2007.
- [25] L. Halpern, C. Japhet, and J. Szeftel. Optimized Schwarz waveform relaxation and discontinuous Galerkin time stepping for heterogeneous problems. *SIAM J. Numer. Anal.*, , 50(5):2588–2611, 2010.
- [26] X. Antoine and E. Lorin. On the rate of convergence of schwarz waveform relaxation methods for the time-dependent Schrödinger equation. *J. Computational and Applied Mathematics*, 354:15–30, 2019.
- [27] D. S. Daoud and D. Subasi. A fractional splitting algorithm for nonoverlapping domain decomposition for parabolic problem. *Numer Methods Partial Differential Eq.*, 18(5):609–624, 2002.
- [28] L. Zhu, G. Yuan, and Q. Du. An explicit-implicit predictor-corrector domain decomposition method for time dependent multi-dimensional convection diffusion equations. *Numer. Math. Theor. Meth. Appl.*, 2(3):301–325, 2009.
- [29] M. Eisenmann and E. Hansen. Convergence analysis of domain decomposition based time integrators for degenerate parabolic equations. *Numerische Mathematik*, 140:913–938, 2018.
- [30] M. J. Gander, L. Halpern, C. Japhet, and V. Martin. Viscous problems with inviscid approximations in subregions: a new approach based on operator factorization. *ESAIM: Proceedings*, 27:272–288, 2009.
- [31] G. Starius. On composite mesh difference methods for hyperbolic differential equations. *Numerische Mathematik*, 35:241–255, 1980.

- [32] M. J. Berger. On conservation at grid interfaces. *SIAM J. Numer. Anal.*, 24:967–984, 1987.
- [33] H.S. Tang, R.D. Haynes, and G. Houzeaux. A review of domain decomposition methods for simulation of fluid flows: Concepts, algorithms, and applications. *Arch Computat Methods Eng*, 2020.
- [34] E. Pärt-Enander and B. Sjögreen. Conservative and non-conservative interpolation between overlapping grids for finite volume solutions of hyperbolic problems. *Computers & Fluids*, 23:551–574, 1994.
- [35] H. S. Tang and T. Zhou. On nonconservative algorithms for grid interfaces. *SIAM J. Numer. Anal.*, 37:173–193, 1999.
- [36] H.S. Tang and F. Sotiropoulos. Fractional step artificial compressibility schemes for the unsteady incompressible Navier–Stokes equations. *Computers & Fluids*, 36:974–986, 2007.
- [37] Z. L. Wu. On uniqueness of steady state solutions for difference equations on overlapping grids. *SIAM J. of Numer. Anal.*, 33(4):1336–1357, 1996.
- [38] H. S. Tang, D. L. Zhang, and C. H. Lee. Comments on algorithms for grid interfaces in simulating Euler flows. *Comm. Nonlinear Science and Numerical Simulation*, 1:50–54, 1996.
- [39] G. Houzeaux and R. Codina. An iteration-by-subdomain overlapping Dirichlet/Robin domain decomposition method for advection–diffusion problems. *J. Computational and Applied Mathematics*, 158:243–276, 2003.
- [40] M. J. Gander and A.E. Ruehli. Optimized waveform relaxation methods for RC type circuits. *IEEE Transactions on Circuits and Systems I: Regular Papers*, 51(4):755–768, 2004.
- [41] Y. Saad. *Iterative Methods for Sparse Linear Systems, 2nd ed.* SIAM, 2003.
- [42] S. V Patankar. *Numerical heat transfer and fluid flow.* Hemisphere Publishing Corporation, 1980.
- [43] H. K. Versteeg and W. Malalasekera. *An Introduction to Computational Fluid Dynamics: The Finite Volume Method.* Pearson Education Limited, 2007.
- [44] J. B. Scarborough. *Numerical Mathematical Analysis, 1st edition.* The Johns Hopkins Press, 1930.
- [45] J. B. Scarborough. *Numerical Mathematical Analysis, 5th edition.* The Johns Hopkins Press, 1958.
- [46] J. F. Epperson. *An Introduction to Numerical Methods and Analysis, 2nd edition.* Wiley, 2013.
- [47] L. Ge and F. Sotiropoulos. 3D unsteady RANS modeling of complex hydraulic engineering flows. I: numerical model. *J. Hydraul. Eng.*, 131:800–808, 2005.
- [48] M. J. C. Gover. The eigenproblem of a tridiagonal p-toeplitz matrix. *Linear Algebra and its Applications*, 197,198:63–78, 1994.
- [49] M. J. Gander and H. K. Zhao. Overlapping schwarz waveform relaxation for the heat equation in n dimensions. *BIT Numerical Mathematics*, 42(4):779–795, 2002.
- [50] J. Stewart. *Multivariable Calculus: Concepts and Contexts.* Thomson Brooks/Cole, 2005.